Magnetic Surface Levels in Cu—Observation and Analysis of Microwave Resonances and Determination of Fermi Velocities

R. E. Doezema and J. F. Koch
Department of Physics, University of Maryland, College Park, Maryland 20742
(Received 5 October 1971)

The resonance spectra of magnetic-field-induced surface states are studied in fields in the range 0—250 Oe at 36 GHz in high-purity Cu single crystals. Using the known Fermi-surface geometry of Cu, we identify the locations of the resonant electrons on the Fermi surface. We carefully consider the resonance line shape to interpret the observed dR/dH (field derivative of the real part of the surface impedance) peak positions and determine the Fermi velocity point by point along the central zones in the (100) and (110) planes. Various types of surface perturbations and their effect on the line shapes of the resonances are discussed, together with some considerations of the effect of tipping the field out of the sample plane.

I. INTRODUCTION

Magnetic-field-induced surface-state resonances[1-4] have in the past few years evolved from the realm of curious low-field structure in the surface impedance of metals[5,6] to a well-understood solid-state phenomenon. Detailed experimental studies[4,7] of these surface states, which correspond to electrons moving in skipping trajectories along the surface, have previously been carried out in metals and semimetals where the resonances were assigned to small cylindrical portions of Fermi surface (FS), i.e., those electrons most seriously perturbed by the lattice potential. In Cu, however, the observed resonances are due to "honest" metallic electrons on spherelike sections of FS. The identification of these electrons is made possible by knowledge of the shape of the Cu FS and is facilitated by an at least rough idea of the electron velocity variation over the FS. The identification of the location on the FS of the resonant electrons is crucial in obtaining a measure of the velocity and scattering rates at points on the FS. We present here the results of a study of the surface-electron resonances in Cu and the velocity information derived from them. We explore the dependence of the resonances on field tipping and surface condition, and examine a situation where the surface-state signals provide FS geometry information. A separate publication is intended to elaborate on a preliminary report[8] on the electron-phonon scattering rates in Cu.

II. EXPERIMENTAL NOTES

As in cyclotron resonance experiments, the samples form a wall of a resonant cavity. Using a conventional microwave spectrometer, we measure the field derivative of the real part of the surface impedance, dR/dH, as a function of the applied magnetic field at a fixed microwave frequency. Details concerning the apparatus and techniques are amply described elsewhere.[6,7]

The Cu samples used in the experiments were spark cut from large single-crystal boules grown by the Czochralski method. The starting material, nominally 99.999% pure, was obtained from the American Smelting and Refining Co. The samples were subsequently annealed in a partial oxygen atmosphere (4×10^{-4} Torr) at 1000 °C for about 5 days. The resulting residual resistivity ratio of the samples ranged from 10 000 to 40 000.

After lapping, the samples were electropolished in a 2:1 solution of orthophosphoric acid and water according to a procedure quoted by Tegart.[9] Since specular reflection of the electrons at the surface is necessary for the existence of surface-state resonances, proper surface preparation is an essential ingredient for successful experiments. Tegart recommends about 30 min of polishing time, but we find that ten or more hours are desirable to give the best resonance spectra. In addition, care must be taken to thoroughly wash the samples after polishing to remove any acid residue.

III. SURFACE-IMPEDANCE CALCULATIONS AND THE GEOMETRY OF THE Cu FERMI SURFACE

Microwave transitions between the quantized surface levels give rise to a spectrum of dR/dH resonance peaks as a function of applied magnetic field H. The field positions of the resonances allow a determination of the parameter $(K/v_F^3)_\perp$; here K is the radius of curvature on the FS for the resonant electrons and v_F their velocity, and $\perp$ designates components of these quantities in the plane normal to the magnetic field. In this section we discuss how one obtains $(K/v_F^3)_\perp$ by fitting the experimental spectra to a calculation of dR/dH, and how to determine the points on the FS which contribute the resonant electrons.

A. Line Shapes

Calculations of the surface-impedance resonances

have been made by Nee, Koch, and Prange (NKP)[2] for the case of cylindrical FS. For perfectly specular reflection at the surface, the line shapes and the positions of peaks in the dR/dH resonance spectrum are found to depend on three fitting parameters: β, $\Gamma^* = 1/\omega\tau$, and $(K/v_F^3)_\perp$. Here

$$\beta = \frac{1}{(2\omega)^{1/2}} \left(\frac{v_F}{K}\right)_\perp^{1/2} \frac{1}{\delta} , \tag{1}$$

where ω is the microwave frequency, δ the anomalous-skin-effect (ASE) skin depth, and τ the electron relaxation time. The resonance condition[1] is given by

$$H_{mn} = (\hbar/e)\,\omega^{3/2}\,(a_m - a_n)^{-3/2}\,(2K/v_F^3)_\perp^{1/2} , \tag{2}$$

where a_m is the mth root of the Airy function. NKP find that for the dominant peaks the resonance condition is satisfied at the dR/dH maximum to within a few percent. For the most part, therefore, the parameter $(K/v_F^3)_\perp$ determines the position of the resonances whereas Γ^* and β determine their widths and relative amplitudes. By fitting the proper β and Γ^* and by taking into account deviation from the cylindrical FS geometry (k_H broadening—k_H being along the field direction in reciprocal space), we calculate the corrections to the resonance condition in order to interpret the dR/dH maxima more exactly.

In practice we concentrate on the $m = 2$, $n = 1$ transition which, for the values of β and Γ^* observed experimentally, has the largest amplitude. The resonance factor $(a_2 - a_1)^{-3/2}$ has the value 0.432, but the dR/dH peak position H_p will generally appear shifted by a few percent from the value H_{21}. The magnitude of the shift depends on the values of β and Γ^*, as well as the k_H broadening effect.

To explore the k_H broadening effect we consider a section of Cu FS for which the calculation can be done exactly—the neck oriented normal to the surface in a (111)-plane sample. The neck has the form of a hyperboloid with a circular cross section. As in Fig. 1, the skipping electrons lie on a narrow belt centered about the line $v_z = 0$. The skipping angle, i.e., the width of the $v_z = 0$ belt, is on the order of 1 deg, measured with respect to the neck center. Thus the trajectory between reflections from the surface can be taken as part of a circle, with curvature equal to the value at the $v_z = 0$ point. Along the effective zone $K_\perp$ varies as $K_0 \cos\theta$ and $v_{F\perp}$ as $v_F \cos\theta$, where θ is the angle the normal to the FS makes with the x axis. H is taken to lie along the y axis. K_0 is the perpendicular radius of curvature at $\theta = 0$, and we have assumed a constant v_F around the zone (justified below). Thus along the zone, $(K/v_F^3)_\perp^{1/2}$ varies as $(K_0/v_F^3)^{1/2}/\cos\theta$. This variation in the resonance parameter produces the k_H broadening. Just as is the case for a k_H-dependent mass in cyclotron resonance, the major contribution to the surface-state resonance is due to electrons with the extremal value of the resonance parameter. The calculation proceeds by cutting the $v_z = 0$ belt into cylinderlike sections with axes along $\vec{H}$, and adds up the appropriate contributions of each of the cylinders.[7] This process is relatively simple for constant β and Γ^* along the $v_z = 0$ zone as is the case for our prototype neck. The spectrum for each segment is just that of the central cylinder [for which $(K/v_F^3)_\perp$ is an extremum], but is scaled up in field by the increase in $(K/v_F^3)_\perp^{1/2}$ and adjusted in amplitude by a factor that accounts for the relative number of trajectories and their coupling to the rf field.

The k_H sum to be performed is

$$\frac{dR}{dH} \propto \sum_n \Delta k_{Hn} v_x(k_{Hn})\,\gamma(k_{Hn})\,F\,(\gamma(k_{Hn})H;\ \beta;\ \Gamma^*) , \tag{3}$$

where k_{Hn} denotes the k_H coordinate of the nth cylindrical segment. The rf current is taken to be in the x direction. $\gamma(k_{Hn})$ is the scale factor for the normalized field h, i.e.,

$$h = \frac{e}{\hbar}\left(\frac{v_F^3}{2K}\right)_\perp^{1/2} \omega^{-3/2}\, H = \gamma H . \tag{4}$$

The function F represents the dR/dH spectrum calculated for a cylinder and scaled to proper field according to the value of γ.

Rewriting Eq. (3) in terms of θ, we have

$$\frac{dR}{dH} \propto \sum_n \Delta\theta_n \cos\theta_n v_x(\theta_n)\,\gamma(\theta_n)\,F(\gamma H;\ \beta;\ \Gamma^*) , \tag{5}$$

which for our neck case reduces to

$$\frac{dR}{dH} \propto \sum_n \Delta\theta_n \cos^3\theta_n F(\gamma H;\ \beta;\ \Gamma^*) . \tag{6}$$

The identical result is obtained for spherical FS geometry. In carrying out the summation we use

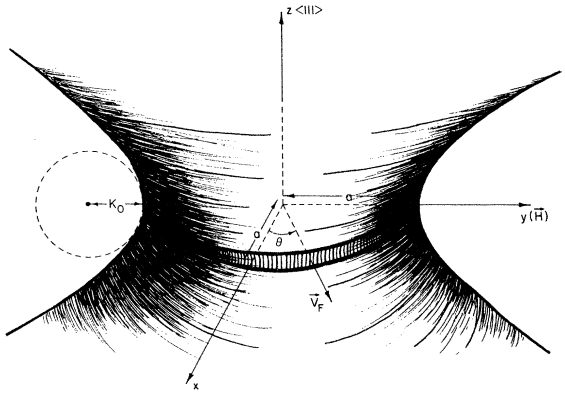

FIG. 1. Neck on the Fermi surface of Cu with the zone of skipping electrons.

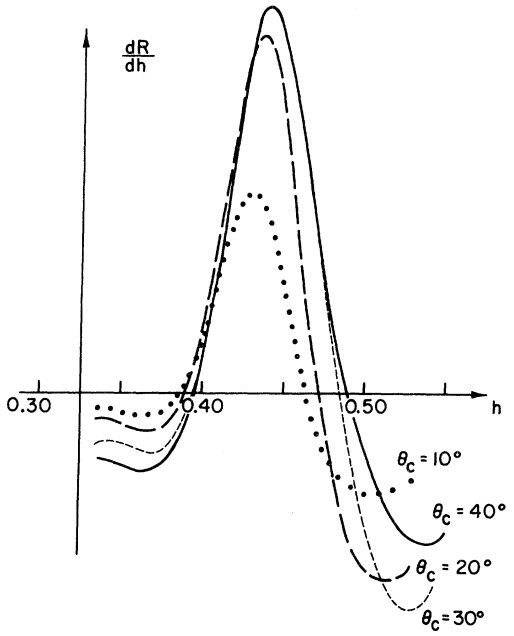

FIG. 2. Calculated lines for the $1 \rightarrow 2$ transition for select values of angular length of the skipping electron zone.

intervals of constant width $\Delta\theta_n$.

In order to examine how electrons resonating near the extremum in $(K/v_F^3)_\perp^{1/2}$ contribute to the observed dR/dH signal, we carry out the summation to various values of a cutoff angle $\theta = \theta_c$. The change in the line shape of the $1 \rightarrow 2$ transition as θ_c is varied is seen in Fig. 2. The calculation is for representative values of $\beta = 0.5$ and $\Gamma^* = 0.075$. The line increases in amplitude as more and more "cylinders" contribute, and broadens asymmetrically as the $(K/v_F^3)_\perp^{1/2}$ parameter increases the field location of each cylinder contribution as $1/\cos\theta$.

It is evident from the figure that the product of line amplitude and width, which is a measure of the absorption strength, does not saturate until $\theta_c \simeq 35°$; that is, electrons on a segment of the $v_z = 0$ belt extending 35° on both sides of $\theta = 0$ contribute significantly to the final line shape. The peak position h_p and relative linewidth at half-amplitude[10] $\Delta h/h_p$ are plotted as a function of θ_c in Fig. 3. The solid line gives the results for the neck. Comparing these with a cylindrical FS calculation ($\theta_c \rightarrow 0°$), we find that at saturation ($\theta_c \approx 35°$) the width has increased by 30% and peak position has shifted from 0.428 to 0.439. To explore how the broadening and shift depend on the details of the FS model, we examine in Fig. 3 two other examples. The first of these (light dash line) weights each cylindrical segment equally but retains the anisotropy $\gamma(k_H)$ for the neck model; i.e., we replace $\cos^3\theta_n$ by $\cos\theta_n$ in Eq. (6). The second model simulates a more rapid variation in $\gamma(k_H)$. In the function F, γ is taken to vary as $\cos 2\theta_n$ in place of $\cos\theta_n$ while the factor $\cos^3\theta_n$ is retained in the summation of Eq. (6). The increased anisotropy leads to saturation at lower values of θ_c as is evident from the heavy dash line in the figure. The final linewidth and peak position values also depend on the details of the FS model.

The peak position h_p varies also with the choice of values for β and Γ^*. We have computed the cylinder spectra for a number of β and Γ^* combinations. The resulting peak positions are plotted in Fig. 4. For the special case $\beta = 0.50$, we show a curve which includes spherical k_H broadening. It becomes clear that unless β, Γ^*, and FS anisotropy are quite accurately known, h_p and hence the calculated v_F are uncertain. Evidently this uncertainty is minimal when Γ^* is small. In that limit the dR/dH peak occurs at the field H_{21}, as defined in Eq. (2), regardless of the β value or FS anisotropy.

With the exception of signals from the ⟨110⟩ point (where the term ⟨110⟩ point is taken to mean the point where the ⟨110⟩ axis intersects the Fermi

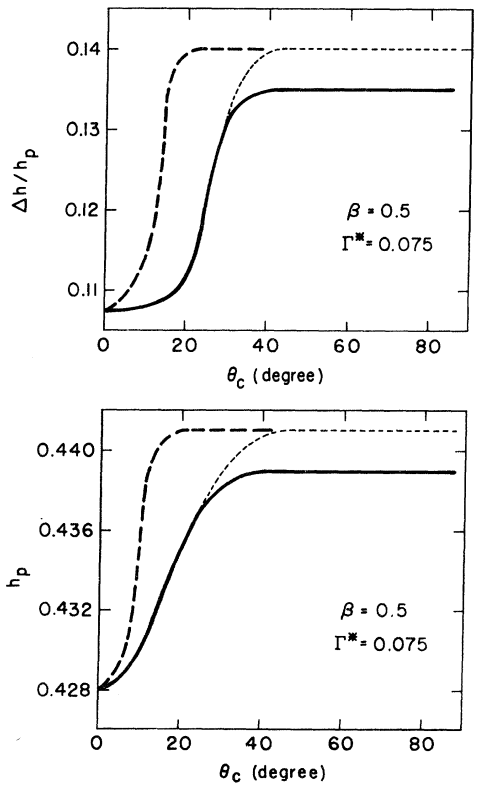

FIG. 3. Fractional half-width and peak position of the $1 \rightarrow 2$ transition vs angular length of the skipping electron zone. The solid curves correspond to the neck case or to a spherical Fermi surface and the dashed lines to variations discussed in the text.

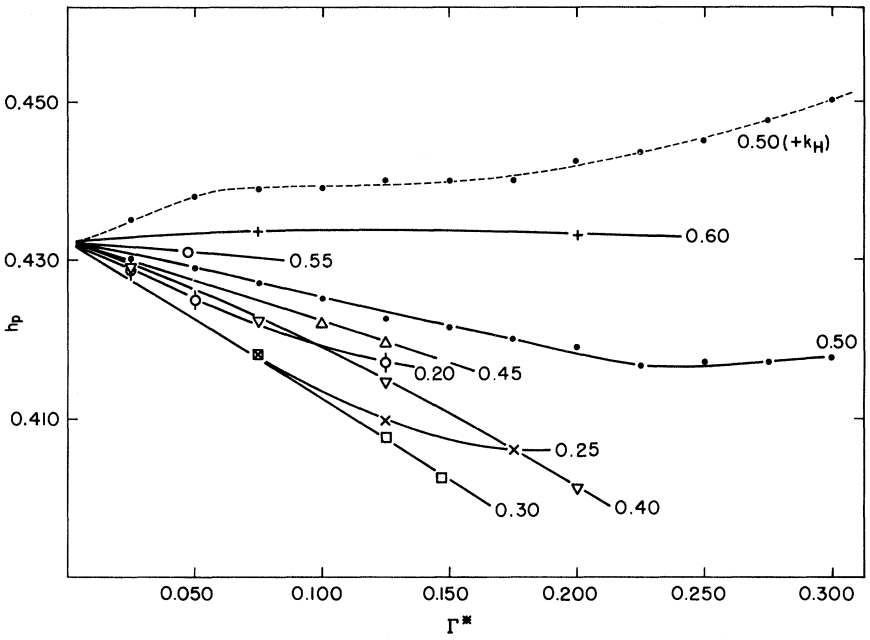

FIG. 4. Calculated peak positions (1 → 2) in normalized field units vs Γ^*, for various values of β. The dashed curve includes the correction due to k_H broadening.

surface), data used in obtaining velocities have Γ^* values ranging from 0.025 to 0.05, and β values in the range 0.4–0.55. Admittedly the exact k_H anisotropy is different for each experimental point, but for most cases it is such that the extremal value of the resonance parameter is a minimum with a more or less parabolic variation about this value. Thus the spherical k_H broadening that applied in the neck case can be taken as characteristic of most of the data. The different curves of Fig. 3 give us a measure of the probable uncertainty that results from this simplification. For $\Gamma^* = 0.025$ we therefore find that with k_H broadening, h_p ranges from 0.433 to 0.436, and for $\Gamma^* = 0.05$ from 0.433 to 0.439. For the interpretation of the resonance peaks in Cu, the representative value of $h_p = 0.435$ has been chosen when the extremal value of the resonance parameter is a minimum. In view of the foregoing discussion, we expect this value to be correct to about 1%. We also note that in our experiments on the temperature dependence of the resonance,[8] there is not observed any significant shift of h_p with Γ^* between 0.025–0.15. This result is expected from the curve of Fig. 4 with $\beta = 0.50$ and k_H broadening included. By contrast, recent data in Bi for which β is on the order of 0.4 shows a distinct downward shift in peak position with increasing Γ^*.

We return now to a consideration of the resonance spectrum of the neck model. Figure 5 compares calculated and experimental curves. $\Gamma^* = 0.0212$ is chosen to match experimental peak widths, and $\beta = 0.50$ gives the best fit to the observed peak-amplitude ratios. The uncertainty in the choice of β is about 10%. In normalized field units, the 1 → 2 transition peak falls at $h_p = 0.434$. The calculated curve achieves a satisfactory fit to the experimental

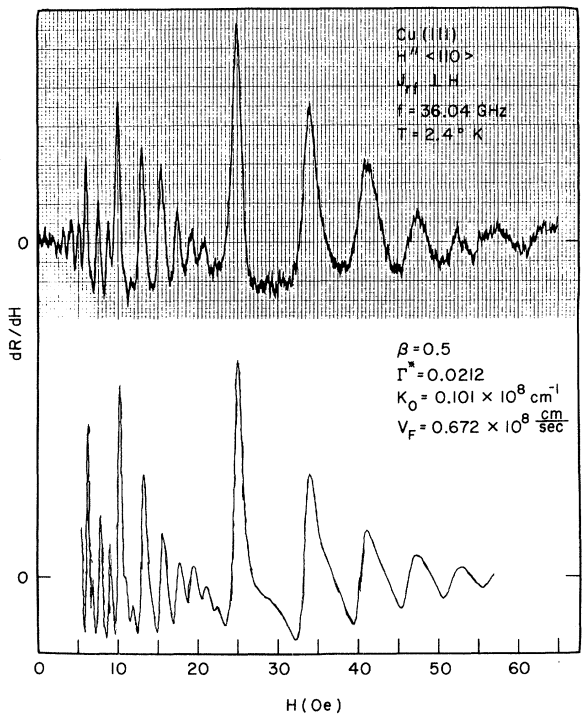

FIG. 5. Comparison of the experimental resonance spectrum (upper trace) with the calculated spectrum (lower trace) for the neck geometry. The dominant resonance at 25 Oe is the 1 → 2 transition. (dR/dH units are arbitrary.)

trace. We shall have occasion to discuss remaining discrepancies in a later section.

B. Fermi-Surface Considerations

The preceding discussion concerned itself with the question of how to extract from the experimental traces an extremal value of $(K/v_F^3)_\perp$. To complete the interpretation of the signals we must next raise the question of where on the $v_z = 0$ zone the measured value applies, i.e., to locate the resonating electrons. For certain high-symmetry directions of the magnetic field we can make an *a priori* identification of the location of the $(K/v_F^3)_\perp$ extrema, but in general a considerable amount of computational effort is required. The effective point could, in principle, be located experimentally making use solely of the known FS geometry. One could measure signal amplitude as a function of the direction of the linearly polarized rf currents. An amplitude maximum occurs at such angle where the current direction coincides with $\vec{v}_F$ on the zone $v_z = 0$. For sufficiently simple FS geometry, this would yield a unique point. In the present experiments we proceed in a different manner, making use of an iterative calculational scheme that both identifies the location of resonating electrons and derives an experimental velocity value for them.

We describe the Cu FS geometry in terms of the analytical expression derived by Halse[11] from de Haas–van Alphen (dHvA) data. Halse estimates radius vectors of his surface to be correct to 0.2%. The FS geometry obtained by Lee[12] using an independent analysis of dHvA data agrees with Halse's work and would serve as an equally good starting point. In any case, both $K_\perp$ and the direction of v_F along the $v_z = 0$ zone are known to sufficient accuracy. In principle, the iteration scheme now proceeds as follows. Along the zone we postulate some arbitrary but reasonable distribution of v_F values, possibly some constant value. For each direction of H we now obtain the location of the $(K/v_F^3)_\perp$ extremum and thus assign observed resonance signals to specific locations on the FS. Thus experimentally measured H_p value together with the $K_\perp$ for that location yields a value for the velocity of these particular electrons which, in general, is different from the initially assumed value. The new values obtained in this fashion define a new v_F anisotropy along the zone which, in turn, serves for the next iteration. We recompute the location of extremal values, to find yet another velocity distribution. As we shall illustrate below, the process converges so rapidly that after only a few iterations experimental and calculated resonance fields agree. The iteration scheme is made even easier by using [as we do for the case of the (110) zone] the v_F plots derived by Lee[13] from an analysis of cyclotron resonance data, for the most part that of Koch, Stradling, and Kip.[14] After the iterations we arrive at a point by point plot of v_F on the FS which, together with the FS geometry of Halse, is exactly consistent with the observed surface-electron resonance.

In concluding this section on the analysis of the data, we draw attention again to the fact that an accurate knowledge of FS geometry is a prerequisite to the kind of detailed study of surface-electron resonances that we present here. While in principle $K_\perp$ can be measured from the curvature shift,[15] in practice for a complete program this would be quite tedious and yield less accurate curvature values than those available from analysis of dHvA effect data.

IV. EXPERIMENTAL RESULTS, ANALYSIS, AND DISCUSSION

In this section we present data on surface-electron resonances in four sample planes of Cu. We describe the field positions of observed peaks and examine their anisotropy with field direction. We use the iteration scheme outlined above to identify the location of resonant electrons on the FS and to obtain values of their velocity.

A. Experimental Data

1. (100) Plane

In Fig. 6 values of H_p (the magnetic field position of the $1 \rightarrow 2$ resonance transition) are plotted against θ, the angle the field H makes with the $\langle 100 \rangle$ direction in the sample plane. For $H \| \langle 100 \rangle$, two series of resonances are observed: one with H_p at 22.7 Oe, the other at 56.9 Oe. The first of these is observed most strongly with microwave currents J_{rf} polarized perpendicular to H, whereas the 56.9-Oe peak is strong when the polarization direction is nearly parallel to H, indicating that the velocities of the two groups of resonant electrons are nearly perpendicular. Upon rotation of H away from $\langle 100 \rangle$, the 22.7-Oe peak moves slowly up in field (a-c in Fig. 6), whereas the 56.9-Oe peak immediately splits: one branch (b'-d) rising steeply in field, the second (b-c') descending to merge with the a-c branch at $\theta = 45°$.

We next wish to examine the question of how to identify resonant electrons on the Fermi surface. Figure 7 shows for example the spectrum observed along $\langle 100 \rangle$ in the (100) plane with currents aligned perpendicular to H. In addition to the major series with H_p near 23 Oe, the weak resonance near 57 Oe is evident for this polarization. The fact that the 22.7-Oe resonance shows no splitting with rotation of H away from $\langle 100 \rangle$ is sufficient for an *a priori* identification of the resonant electrons. Without prior knowledge of the variation of v_F along the $v_z = 0$ zone, it is evident that such a resonance is

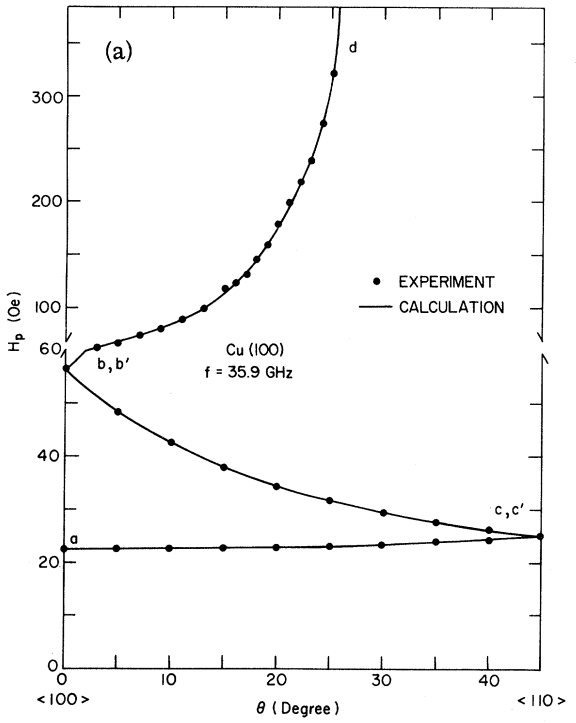

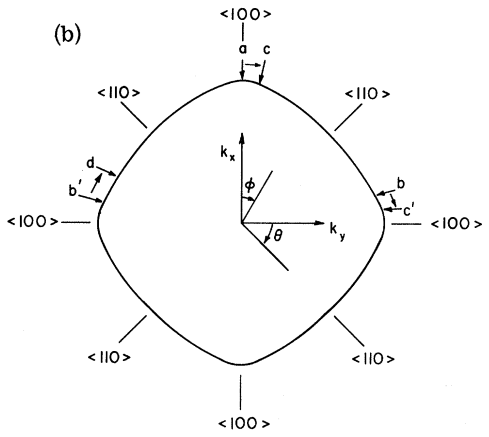

FIG. 6. (a) Anisotropy of $1 \rightarrow 2$ resonance positions in the (100) sample plane of Cu vs θ the angle between the field direction and the $\langle 100 \rangle$ axis. (b) Corresponding locations of the resonant electrons on the central (100) zone of the Cu Fermi surface.

due to a single point centered at $\phi = 0°$, i.e., in this case the $\langle 100 \rangle$ point marked a in Fig. 6. For this point, the observed H_p value together with Halse's value of the curvature radius $K = 0.3731 \times 10^8$ cm^{-1}, yields a Fermi velocity of $v_F = 1.11 \times 10^8$ cm/sec.

The resonance b, b' in Fig. 6, where splitting is observed with field rotation about the symmetry direction, must arise from equivalent $(K/v_F^3)_\perp^{1/2}$ extrema located symmetrically about $\phi = 0°$. Knowledge of their exact location requires a computation of the resonance field H_{21} as a function of position angle θ in the Fermi surface and presupposes knowledge of both K and v_F along the zone. Using the velocity values derived below, we compute the H_{21} variation indicated in the insert of Fig. 7. The minima at $\phi = 0°$ and $\phi = \pm 77.2°$ identify the location of resonance electrons, and simultaneously yield H_p values to be compared with experiment.

For other field directions in the (100) plane the peak positions are calculated in the same way and are given by the solid line in Fig. 6. The letter labels of the points correspond to the branches showing how each point moves as H is rotated. From the experiment on the (100) plane we learn about only those electrons located within the ranges a–c, b–c', and b'–d.

2. (110) Plane

The anisotropy plot of the (110) plane in Fig. 8 is considerably more complex than that of the (100) plane. Nevertheless, the movement of the peak positions with field direction has been unraveled from the experimental traces, and the resonant electrons corresponding to the various branches are indicated in the figure. Again the solid lines give calculated peak positions to be compared with the experimental points.

Points a and e, observed respectively with H along $\langle 110 \rangle$ and $\langle 100 \rangle$ are examples of *a priori* identification as already discussed for the (100) plane. The a point provides no new information since it is the same $\langle 100 \rangle$ point seen in the (100) plane. The resonance appears at exactly the same field since $K_\perp$ is unchanged from its (100)-plane value, i.e., the FS is locally spherical in the vicinity of the $\langle 100 \rangle$ point. The spectrum corresponding to the point e, in fact to the whole branch e-j, is observed experimentally only at temperatures between about 10 and 25 °K because at lower temperatures the d, d' and f, f' spectra mask the e series. At the higher temperatures, the e series emerges because the scattering rate for the e point increases much less rapidly than for the other points. The e spectrum is also unusual in that its β value is only about 0.25. The assignment of β and Γ^* values for this series is more uncertain because of the relatively weak resonance signals. Calculations show that for low β values the $2 \rightarrow 3$ transition has the largest peak amplitude. We have consequently determined the $1 \rightarrow 2$ peak position (as plotted in Fig. 8) by measuring the $2 \rightarrow 3$ peak position and scaling by the factor 0.740. The Γ^* value is fit as 0.075 and thus the cylinder calculation gives $h_p = 0.418$ (see Fig. 4). The parameter $(K/v_F^3)_\perp$ is a maximum at point e for $H \parallel \langle 100 \rangle$; hence, k_H broadening is expected to give a correction down from 0.418. Assuming this correction is as large as the up

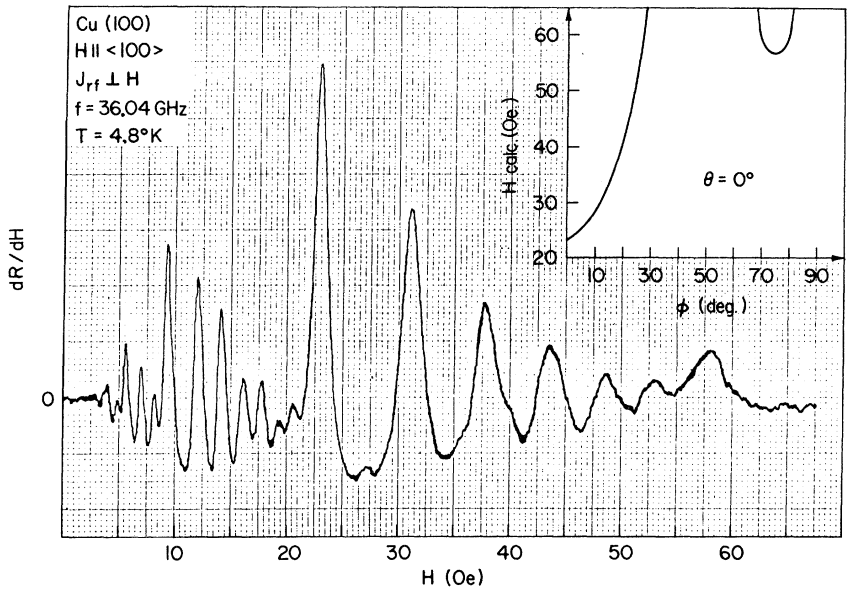

FIG. 7. Surface-state resonance spectrum in the (100) plane of Cu. The insert gives the calculated $1 \rightarrow 2$ resonance field along the zone of skipping electrons; the minima in this plot correspond to the field positions of the two $1 \rightarrow 2$ resonances observed.

correction for a resonance parameter minimum, we obtain $h_p = 0.408$. With these adjustments and making use of the measured $2 \rightarrow 3$ peak position of 60.0 Oe at 35.90 GHz, we arrive at $H_p = 44.4$ Oe for the $\langle 110 \rangle$-point resonance. Using $K = 1.623 \times 10^8$ cm^{-1} as obtained from Halse's geometry, we obtain $v_F = 1.11 \times 10^8$ cm/sec. Because of relatively weak signals and consequent uncertainty in the values of β and Γ^*, the possible error in this velocity value is larger than for most other orientations.

Before concluding the discussions on the (110)-plane data, we again consider the $\langle 110 \rangle$ direction spectrum to illustrate that very careful, painstaking analysis is required to identify the resonant electrons. Figure 9 shows the data for $H \parallel \langle 110 \rangle$. The a peak, as mentioned earlier, is readily identified as due to the $\phi = 0°$, $\langle 100 \rangle$-point electrons. Two other resonances b and c are identifiable in the data. As the insert shows, these are expected from two additional extrema in the resonance parameter at values of $\phi = 24.0°$ and $39.3°$. As a final point, we show in Fig. 10 data for which the current direction is aligned parallel to H and along $\langle 100 \rangle$. Previous discussions of surface-electron resonances envisioned cylindrical FS models and emphasized that optimal data were obtained in the perpendicular polarization mode. The resonances f, f' (see Fig. 8) involve electrons whose velocity is directed nearly parallel to $\langle 100 \rangle$, and they consequently are seen best in the $H \parallel J_{rf}$ configuration. The spectrum in Fig. 10 shows no trace of resonances e and d, d' which are inhibited by the polarization.

3. (111) Plane

The (111)-plane spectrum is dominated at all magnetic field directions by signals from neck electrons as sketched in Fig. 1. There is not observed any anisotropy of this signal as the field is rotated. Additional weak resonances with considerable anisotropy are presumably due to other $v_z = 0$ zones, but could not readily be interpreted because our computation method, in which the FS geometry is expressed as a cubic equation, is not applicable in this plane. The neck-electron signal is that shown previously in Fig. 5.

The isotropy of the neck spectrum with field direction is easily understood on the basis of the Halse FS which predicts a constant curvature radius around the neck, $K_0 = 0.101 \times 10^8$ cm^{-1}. The constant peak position then implies a constant velocity, $v_F = 0.672 \times 10^8$ cm/sec.[16] The resonant electrons thus simply follow the field H around the neck as H is rotated, remaining centered at a point 90° from the field direction.

4. (112) Plane

The signals observed in the (112) plane are plotted in Fig. 11. We have not calculated the $(K/v_F^3)_\perp$ distributions for magnetic field directions in the (112) plane. Nevertheless, we can make some progress in identifying the resonant electrons based on the procedure that we have learned in the (100) and (110) planes.

Consider the point labeled a in Fig. 11. This peak is observed most strongly with $H \parallel \langle 111 \rangle$ for $J_{rf} \perp H$ but weakly with a shifted peak position for the other polarization. A very similar anisotropy is observed in the (110) plane about $H \parallel \langle 111 \rangle$ (point g of Fig. 8). The peak positions are identical. We thus identify the resonant electrons as lying on the neck just as in the (110) plane. As the

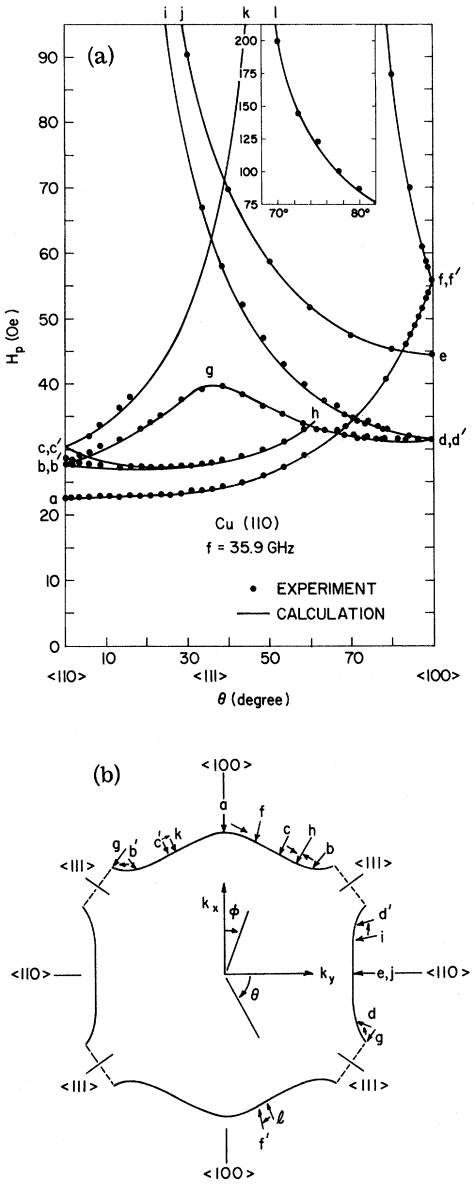

FIG. 8. Anisotropy of $1 \rightarrow 2$ resonance positions in the (110) sample plane of Cu vs θ the angle between the field direction and the $\langle 110 \rangle$ axis. (b) Corresponding locations of the resonant electrons on the central (110) zone of the Cu Fermi surface.

field is rotated to the $\langle 110 \rangle$ axis, the effective point slides off the neck to a point d, which is equivalent to d' for this axis. As expected we observe the splitting of d, d' as H is rotated away from $\langle 110 \rangle$. Peak b in Fig. 11 does not split upon rotation of H away from $\langle 111 \rangle$; thus it can only be attributed to the points b lying on the $v_z = 0$ zones on the out-of-plane necks sketched in the figure. A calculation of the relevant curvature based on the hyperboloid neck geometry (Fig. 1), together with the previously determined v_F on the neck, yields the observed peak position for point b. When H is rotated from $\langle 111 \rangle$ to $\langle 110 \rangle$ the effective point at b slides along the $v_z = 0$ zone to point c which with reference to Fig. 8 lies at $\phi = 64.9°$. The relevant curvature radius of this point we calculate as $K = 0.132 \times 10^8$ cm^{-1}. At $f = 35.90$ GHz, the value of H_p is 25.8 Oe. We consequently obtain the velocity $v_F = 0.720 \times 10^8$ cm/sec for this point. Finally, again from symmetry considerations resonance e can only be assigned to the points near the out-of-plane necks as in the figure.

B. Fermi Velocities

Only for those points on the FS where an *a priori* identification was possible does the data on peak positions directly yield velocity values. To generate both the location of and velocity values for resonant electrons in the more general case, we now resort to the iteration scheme.

We illustrate the general procedure with the (100) plane data. The velocity at both $\langle 100 \rangle$ and $\langle 110 \rangle$ points was found to be equal to 1.11×10^8 cm/sec. As a first approximation we take, as given by the dotted line in Fig. 12, the flat distribution, where all electrons between $\theta = 0°$ and $45°$ are assigned the same value, $v_F = 1.11 \times 10^8$ cm/sec. Using this distribution we compute the positions of the $(K/v_F^3)_\perp$ extrema for each field direction in the (100) plane, thus identifying the locations of the resonating electrons. The $K_\perp$ value at such a point, together with the measured resonance peak field H_p, provides now a new value of velocity for the FS point. After such a first iteration we arrive at the distribution given by the dashed line in Fig. 12. This distribution serves as the starting point of the next iteration, until finally (solid line in Fig. 12) we arrive at a distribution of velocities which is consistent with the data to within experimental error.

For the case of the (110)-plane data, we choose for convenience as the starting approximation the distribution of velocities given by Lee.[13] After these iterations we arrive at velocity values consistent with the data.

Tables I and II provide a summary of the experimentally determined peak positions H_p, together with the velocity values and locations of resonant electrons in the (100) and (110) sample planes. The analysis in Table II has been limited to 5° steps whereas the data (compare Fig. 8) were taken on an even finer grid. Table III and Fig. 13 give a comparison of the velocity values derived by Lee and Halse with those obtained in the present experiments.

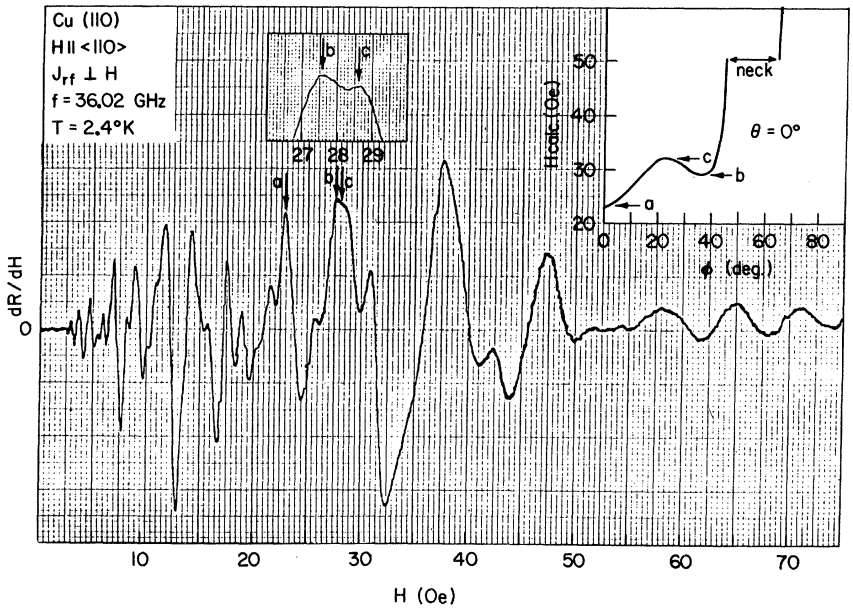

FIG. 9. Resonance spectrum in the (110) plane of Cu as an example of overlapping multiple series of peaks. The 1 → 2 resonances marked correspond to the indicated extrema in the calculated fields vs location on the zone of skipping electrons.

C. Discussion

The agreement between our v_F values which are determined experimentally point by point, and those of Lee and Halse which come from unravelling the orbital velocity averages obtained from experimental cyclotron masses, is in general quite satisfying. To examine to what extent the remaining discrepancies are significant, we consider briefly the uncertainties in our v_F values.

There are three possible contributions to such errors. First, there is the error involved in determining an experimental value of a peak position and microwave frequency. Second, we must consider the uncertainties in fitting the line shapes. Finally, we examine to what accuracy we can locate a point on the FS and the consequent uncertainty in the radius of curvature used to compute v_F.

In determining H_p, the possible calibration error of $\pm 0.3\%$ plays a role. The reproducibility of a given resonance peak has been found to be something like $\pm 0.25\%$, which represents the uncertainties involved in determining the peak position. The microwave frequency is known to an accuracy of $\pm 0.1\%$. We consequently arrive at an estimated

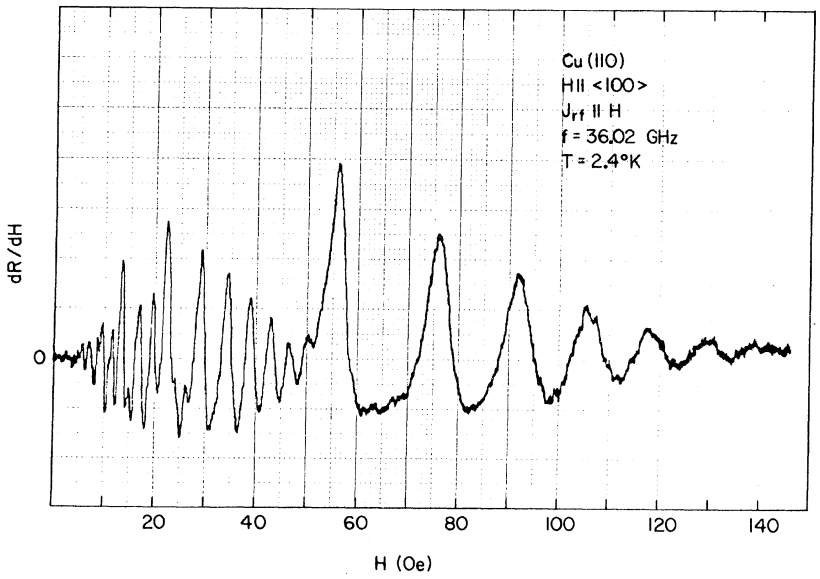

FIG. 10. Resonance spectrum in the Cu (110) plane observed with rf current polarized parallel to the applied field.

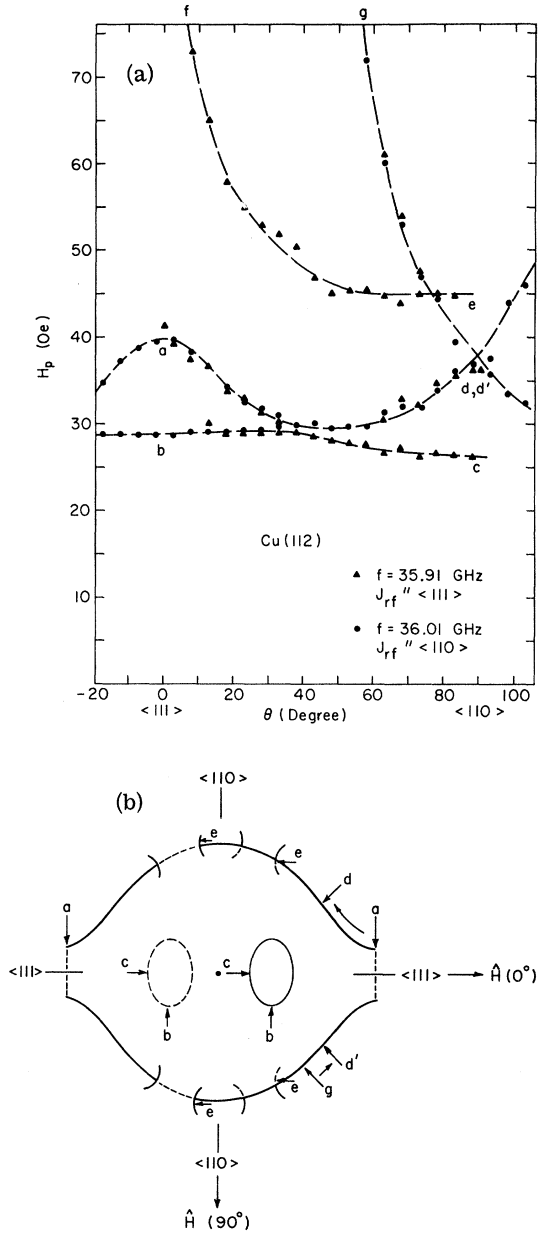

FIG. 11. (a) Anisotropy of $1 \rightarrow 2$ resonance positions in the (112) sample plane of Cu vs θ the angle between the field direction and the $\langle 111 \rangle$ axis. The dashed lines are drawn smoothly through the experimental points. (b) Corresponding locations of the resonant electrons on the zones of skipping electrons for the (112) plane of the Cu Fermi surface.

possible error of $\pm 0.7\%$ in the peak position for a given frequency (recall that $H_p \propto \omega^{3/2}$). In addition, the "true" peak position may also be altered by the presence of an overlapping peak. Only in the (110) plane does this pose a serious problem. Where the peak position was known to be significantly shifted due to overlap, it was not used in the v_F computation. The interpretation of the experimental resonances in terms of the NKP lineshape theory,[2] modified to include k_H broadening, is a very significant factor in determining v_F. As we discussed in Sec. III, the uncertainties in determining the parameters β and Γ^* for the fitting procedure are important since they result in uncertainties in the normalized-field peak position h_p. With the assumption that the theory describes the line shape correctly, the value of h_p is judged reliable to better than $\pm 1\%$. Finally, we consider the contribution of the uncertainty in the FS geometry used in calculating v_F. For the symmetry points, i.e., those with *a priori* identification where we know exactly the location on the FS of the resonant electrons, only the uncertainty in the value of K at that point is important. For the more general case, there is also the uncertainty in the location angle ϕ to be considered. The uncertainty in the value of K comes from two sources. The first is that we have assumed a locally circular orbit. This gives a negligible error since the skipping angle is 1° or less. The second source is the 1° or 2° uncertainty in sample-plane alignment. Together with possible error in location angle ϕ, we estimate that possible error in the

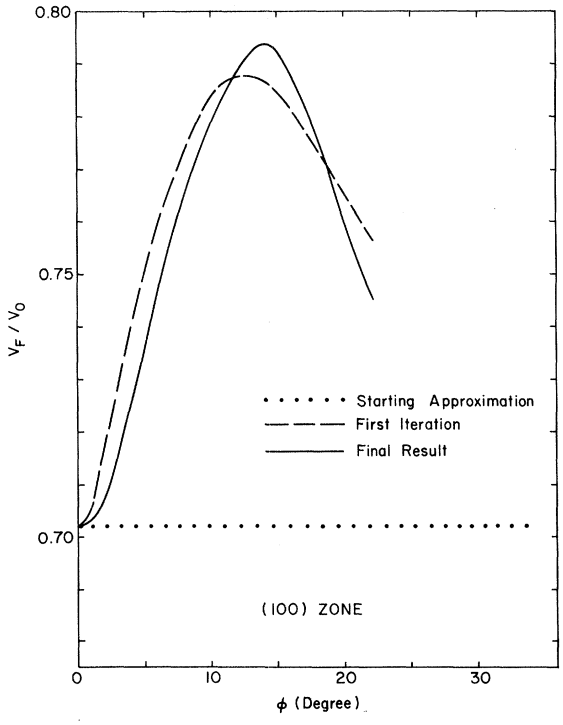

FIG. 12. Velocity values of successive iterations for the (100) zone starting with a constant distribution. The free-electron velocity $v_0 = 1.5779 \times 10^8$ cm/sec. The angle ϕ denotes Fermi-surface locations on the (100) zone relative to the $\langle 100 \rangle$ axis.

TABLE I. Resonance fields and Fermi velocities for the (100) plane in Cu. θ gives the direction of the magnetic field relative to the ⟨100⟩ axis. H_p is the observed $1 \rightarrow 2$ transition peak position at the given microwave frequency. ϕ, measured from the ⟨100⟩ axis, locates the resonant electrons on the Fermi surface.

θ (deg)	H_p(expt) (Oe) ($f = 35.90$ GHz)	ϕ (deg)	v_F (free-electron units: 1.5779×10^8 cm/sec)
0	22.7	0	0.702
	56.9	12.8	0.791
3[a]	63.4	13.3	0.7915
5	22.7	1.15	0.704
	48.6	12.0	0.789
	67.7	13.6	0.799
7	75.1	14.1	0.790
9	82.5	14.3	0.790
10	22.8	2.15	0.709
	43.1	11.05	0.781
11	90.65	14.55	0.794
13	101.9	14.9	0.7935
15	22.9	3.15	0.717
	38.5	10.5	0.777
	117.3	15.3	0.787
16	125.8	15.7	0.787
17	134.8	15.9	0.789
18	147.6	16.4	0.782
19	157.6	16.75	0.786
20	22.9	4.0	0.727
	34.8	9.75	0.778
	178.4	17.25	0.773
21	198.3	17.75	0.767
22	217	18.6	0.772
23	239.5	19.25	0.776
24	273	20.3	0.767
25	23.2	5.2	0.738
	32.1	9.25	0.774
	321	21.8	0.746
30	23.6	6.5	0.752
	30.05	8.6	0.767
35	24.1	6.9	0.755
	28.1	8.2	0.767
40	24.7	7.25	0.7605
	26.5	7.85	0.768
45	25.7	7.55	0.760

[a]The a-c and b-c' branches of Fig. 6 are only tabulated at 5° intervals in θ.

value of K amounts to ±1%.

Combining the uncertainties according to the formula used to calculate v_F, i.e.,

$$v_{F\perp} = \frac{\hbar}{e}\,\omega\left(\frac{h_p}{H_p}\right)^{2/3}(2K_\perp)^{1/3}, \qquad (7)$$

we arrive at an estimated possible error in v_F of ±1.5%. Because of small peak amplitudes observed, the ⟨110⟩ point in the (110) plane is an exception: The increased uncertainty in both H_p and fitting parameters Γ^* and β leads to a net uncertainty of ±3.0%.

As a check on the above error analysis we can examine the internal consistency of our velocity values since there are a number of points on the FS whose velocities are determined in more than one sample plane. The ⟨100⟩ point is observed in both the (110) and (100) planes, and the values of v_F obtained are identical. The neck is common to the (111), (110), and (112) $v_z = 0$ zones, and a resonance due to the neck point occurs in all three planes [at all field orientations in (111), point g of Fig. 8 in (110), and point a of Fig. 11 in (112)]. In free-electron units we have $v_F = 0.426$ from the (111) plane, $v_F = 0.427$ from the (110) plane, and $v_F = 0.428$ from the (112) plane. Another such common point is that at $\phi = 64.9°$ on the (110) zone. The (112) data gives $v_F = 0.456$, whereas we determine $v_F = 0.451$ from the (110)-plane data (free-electron units).

Keeping in mind that the presently derived v_F values have an uncertainty of ±1.5%, we now return to examine the differences apparent in Table III and Fig. 13. Substantial disagreement between our value and those of Halse occurs from $\phi = 0°$ to 5° in the (100) zone and from 0° to 10° in the (110) zone. Disagreement with Lee's values, outside of experimental errors, is in the range 10°–20° in the (100) zone and from about 15°–35° in the (110) zone. Both Lee's and Halse's velocities when integrated according to

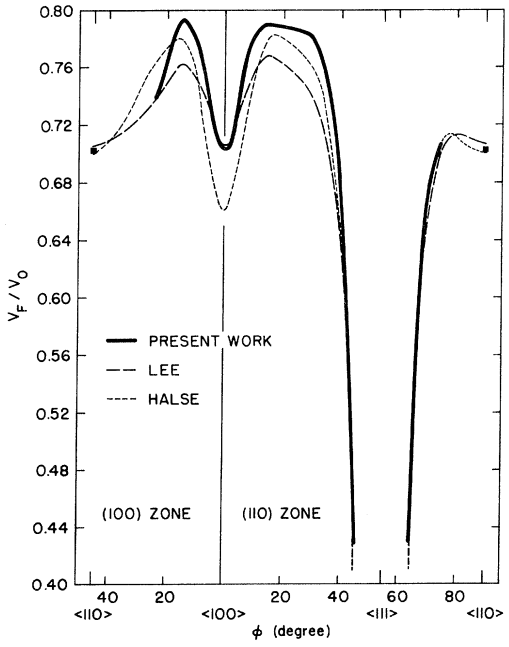

FIG. 13. Fermi velocity for Cu over the (100) and (110) zones. The solid line and the point marked at the ⟨110⟩ axis represent our measured values. The broken curves are taken from Halse (Ref. 11) and Lee (Ref. 13). The free-electron velocity $v_0 = 1.5779 \times 10^8$ cm/sec.

$$m_c = \frac{\hbar}{2\pi} \oint_{\text{orbit}} \frac{dk}{v_F} \qquad (8)$$

(dk is the path-length element) yield the experimentally observed cyclotron masses,[14] and it would be of interest to compare our v_F values in these

TABLE II. Resonance fields and Fermi velocities for the (110) plane in Cu. θ gives the magnetic field direction relative to the ⟨110⟩ axis. H_p is the observed 1 → 2 transition peak position at the given microwave frequency. ϕ, measured from the ⟨100⟩ axis, locates the resonant electrons on the Fermi surface.

θ (deg)	H_p(expt) (Oe) (f=35.90 GHz)	ϕ (deg)	v_F (free-electron units: 1.5779×10^8 cm/sec)	θ (deg)	H_p(expt) (Oe) (f=35.90 GHz)	ϕ (deg)	v_F (free-electron units: 1.5779×10^8 cm/sec)
	22.7	0	0.702		26.3	7.6	0.771
0	27.55	39.3	0.703		30.3	30.2	0.7805
	28.55	~24[a]	···	50	36.2	67.5	0.597
					45.7	71.0	0.6775
	22.8	1.0	0.7025		58.6	90.0	0.698
	27.55	39.4	0.6905				
5	27.95	~24[a]	···		27.75	8.4	0.775
	28.65	39.35	0.698		31.7	28.5	0.784
	31.3	~23[a]	···	55	34.6	67.9	0.614
					41.8	70.7	0.679
	22.8	3.0	0.716		54.8	90.0	0.6975
10	27.45	39.45	0.685				
	30.2	39.4	0.689		29.6	8.8	0.776
	34.1	~23[a]	···		33.4	68.25	0.625
				60	39.0	70.5	0.6775
	22.8	4.0	0.728		51.6	90.0	0.700
	27.3	39.5	0.683				
15	31.9	39.5	0.683		31.7	9.8	0.7805
	37.4	~23[a]	···		32.5	68.7	0.634
				65	36.6	70.45	0.680
	22.9	5.4	0.745		49.2	90.0	0.701
	27.35	39.25	0.691				
20	33.7	39.6	0.682		34.3	10.4	0.784
	41.8	~22.5[a]	···		31.9	68.85	0.6385
				70	34.7	70.4	0.681
	23.0	6.0	0.752		47.2	90.0	0.703
	27.45	37.5	0.717		198.7	17.4	0.7855
25	35.9	39.7	0.682				
	47.5	~22[a]	···		37.8	11.1	0.788
					31.5	69.0	0.643
	23.4	6.4	0.755	75	33.4	70.1	0.6765
	27.55	36.25	0.735		46.0	90.0	0.703
30	38.0	44.6	0.4555		122.0	16.6	0.7835
	90.0	90.0	0.696				
					42.2	11.8	0.787
	23.8	6.8	0.7615		31.4	69.1	0.644
	27.95	33.6	0.761	80	32.4	69.9	0.673
35	63.9	72.2	0.690		45.0	90.0	0.703
	39.6	44.7	0.443		86.9	15.4	0.790
	77.2	90.0	0.704				
					48.1	12.9	0.789
	24.55	7.1	0.762		31.4	69.2	0.6455
	28.55	31.5	0.771	85	31.7	69.7	0.6655
40	39.3	64.45	0.431		45.2	90.0	0.702
	56.0	71.7	0.685		68.4	14.1	0.789
	69.3	90.0	0.702				
					56.1	13.5	0.791
	25.5	7.4	0.7675	90	31.4	69.4	0.656
	29.3	30.75	0.777		44.4	90.0	0.7025
45	37.8	66.25	0.538				
	50.3	71.5	0.682				
	63.3	90.0	0.699				

[a]Approximate FS location: the 1 → 2 peak position is uncertain due to interference from other series; peak is not used for v_F calculation.

TABLE III. Comparison of Fermi velocity values on the Cu Fermi surface. The angle ϕ, measured from the ⟨100⟩ axis, locates the points on the Fermi surface. The errors are as estimated in the works cited.

ϕ (deg)	v_F (free-electron units: 1.5779×10^8 cm/sec) Present work (± 1.5%)	Lee (Ref. 13) (± 1.5 to 2%)	Halse (Ref. 11) (± ~3%)
		(100) zone	
⟨100⟩	0.702	0.704	0.66
5	0.737	0.730	0.70
10	0.777	0.753	0.76
15	0.790	0.762	0.78
20	0.761	0.749	0.77
25	···	0.734	0.76
30	···	0.722	0.74
35	···	0.714	0.72
40	···	0.708	0.71
⟨110⟩	0.702	0.706	0.70
		(110) zone	
⟨100⟩	0.702	0.704	0.66
5	0.742	0.729	0.70
10	0.782	0.757	0.75
15	0.789	0.768	0.78
20	0.788	0.761	0.78
25	0.786	0.752	0.77
30	0.781	0.742	0.76
35	0.749	0.718	0.73
40	0.676	0.645	0.65
neck	0.427[a]	0.413	0.41
65	0.458	0.454[b]	0.45
70	0.670	0.655	0.66
75	···	0.705	0.71
80	···	0.713	0.71
85	···	0.710	0.70
⟨110⟩	0.702	0.706	0.70

[a]An average of the values obtained in the (111), (110), and (112) planes.

[b]Interpolated from Lee's table.

terms. To do so, however, requires that we approximate v_F values in those angular ranges where they could not be measured directly.

If we assume that our velocity curve coincides with Lee's curve in the (100) zone from 22° to 45°, we obtain $m_c = 1.358 m_0$ for the (100) zone. (Here m_0 is the free-electron mass.) For the dog-bone orbit we take our (110)-plane velocity values except in the section $\phi = 75°-90°$, where we assume Lee's values. This yields $m_c = 1.256 m_0$. Koch, Stradling, and Kip[14] measure for the (100) belly orbit, $m_c = (1.370 \pm 0.005) m_0$ and $m_c = (1.290 \pm 0.005) m_0$ for the dog-bone orbit (using Halse's identification for this orbit). Our (100)-zone mass agrees within the experimental errors with the measured mass, but the dog-bone mass does not. In view of the extrapolation between 75° and 90°, however, it does not provide a crucial test. A more meaningful comparison is the case of the neck orbit, since we have measured a constant value of v_F for all points on the orbit. Our value[16] of v_F is 0.427 ± 0.006 (in free-electron units) and represents an average of our measurements in the (111), (110), and (112) planes. With the neck radius of 0.256×10^8 cm^{-1}, we arrive at a mass value of $m_c = (0.440 \pm 0.007) m_0$. Both Lee and Halse derive a neck velocity of 0.413 to agree with the measured cyclotron mass[14] of $m_c = (0.46 \pm 0.02) m_0$. Given the relatively large uncertainty in the neck cyclotron mass, our result is not inconsistent with this value. It does however suggest that the cyclotron mass value for the neck orbit should be somewhat lower. Consideration of the effect of mass broadening (the analog of our k_H broadening) on the measured mass may contribute to such a lowering. In this connection, it is of interest to note that Joseph and Thorsen[17] in dHvA measurements find $m_c = (0.45 \pm 0.014) m_0$. In any case, the neck mass comparison provides a good test of the reliability of our velocity measurements.

In concluding our discussion of the velocity values, we note that for recent Bi experiments[7] the velocity distribution derived from surface-electron resonances is definitely inconsistent with the measured cyclotron mass.[18] The velocity integral was found to yield $m_c = (0.0077 \pm 0.0002) m_0$, which disagrees with the generally accepted value of $(0.0081 \pm 0.0001) m_0$. For Bi, however, the FS geometry is not as well established as that of Cu, and it is conceivable that the discrepancies would be resolved with only minor adjustments in the local curvature radius values.

V. GEOMETRY OF Cu FERMI SURFACE

Our interpretation of the surface-electron resonances in Cu depends on the Halse geometry of the Cu FS. Conversely, the extent to which our observations of the resonance signals agree with the predictions of the Halse model confirms the general features of the FS geometry. In particular, the existence of each resonance series, the angular ranges of these series, and the dependence of their amplitudes on rf current direction conform to the predictions of the Halse geometry.

There is one case, however, where it appears that surface-electron resonances provide a specific test for FS geometry. Both Lee and Halse derive a neck in Cu with exactly circular cross section of radius $K = 0.256 \times 10^8$ cm^{-1}. Recent radio-frequency size-effect (RFSE) data of Perrin *et al.*[19] suggest a scalloped neck with radius vector varying from 0.22×10^8 cm^{-1} at the ⟨112⟩, to 0.29×10^8 cm^{-1} at the ⟨110⟩ in the (111) plane. We have observed neck-electron resonances in several symmetry planes, and all of these are accounted for in terms of the Halse geometry. Specifically the following observations argue against the scalloped-neck model:

(i) The scalloped neck suggests multiple extrema in $(K/v_F^3)_\perp$ in the (111) $v_z = 0$ zone, but only one is observed. In the (110) plane, the model would have multiple $v_z = 0$ zones passing across the neck, so that one expects extra signals not explained by the Halse geometry. No such signals are observed.

(ii) For all field orientations in the (111) plane, the dR/dH resonance peaks due to neck electrons are observed at the same field values. This is exactly consistent with the constant K_0 and v_F predicted by Halse and Lee.

(iii) In the (111) plane, skipping electrons move perpendicular to the plane of the neck. The observed H_p together with the Halse curvature value yields a velocity which must also apply for the (110)- and (112)-plane data where the electrons move in the plane of the neck. Using this velocity value and the in-plane curvature radius of 0.256 $\times 10^8$ cm^{-1}, as given by Lee and Halse, gives the experimentally observed peak positions in the (110) and (112) planes.

(iv) Keeping the direction of the rf currents in the (111) sample plane fixed in an arbitrary direction, we observe upon rotating H that the resonance peak amplitudes fall off as $\cos^2$ of the angle between J_{rf} and the normal to H. This is just the dependence expected for the neck with a circular cross section for constant K_0 and v_F since the velocity vector at the effective point is always normal to H.

Because the resonances always involve both geometry and velocity, we could not, given a particularly malicious variation of velocity in the neck region, unambiguously rule out the scalloped-neck suggestion. Any one of the above observations would not be sufficient, but in sum the observations must be taken to confirm the Lee-Halse geometry and suggest that the RFSE data lead to the wrong conclusion.

VI. FIELD-TILTING EFFECTS

In previous studies[6,7,20] of surface states, tipping of the magnetic field out of the sample plane was generally observed to result in a $1/\cos\theta$ shifting of the resonance-peak positions (θ is the tip angle). The $1/\cos\theta$ tip dependence, together with the similar in plane variation of the peak positions, has been attributed to cylindrical FS geometry.[6,7,21] However, it has recently been shown[22] that, except for the case where $v_z = 0$ zone does not lie in a constant k_z plane, a $1/\cos\theta$ tip dependence is expected for general FS geometry and not just for the special case of a cylinder. This can be understood by considering in the "minimal theory" derivation of Ref. 7 only the Lorentz force component normal to the sample surface, i.e., $F = ev_F H\cos\theta$.

Cu data for the ⟨100⟩-point resonance nicely exemplifies the expected $1/\cos\theta$ variation, for a "locally spherical" FS geometry. Figure 14 shows the variation of the spectrum with tip angle over the range 0°–70°. Peaks are observed to shift exactly as $1/\cos\theta$ to increased field. The relative linewidth $\Delta H/H$ is found to remain nearly constant out to about 50°, and increase rapidly thereafter, as evident from the figure. When the field is tipped the electrons move in a zig-zag path along the $v_z = 0$ zone, sampling varying values of the FS parameters. The broadening is expected to appear as the electron trajectories contributing to a resonance peak traverse an ever larger fraction of the $v_z = 0$

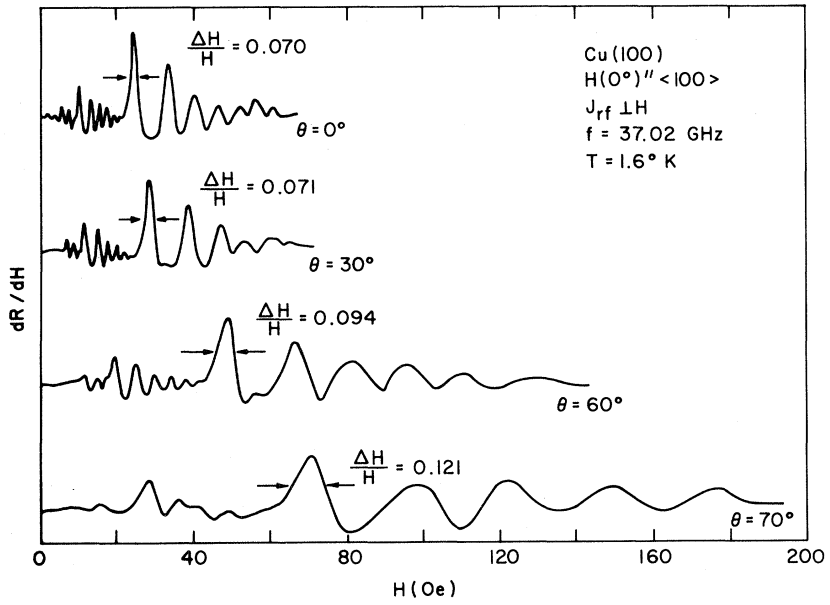

FIG. 14. Variation of the resonance spectrum with tilt angle θ in the (100) plane of Cu.

zone as the tipping angle is increased. The Singhal and Prange calculations[22] predict no appreciable broadening until the tip angle becomes sufficiently large, in qualitative agreement with the data in Fig. 14. The neck geometry in Fig. 1 also satisfies the requirement for a $1/\cos\theta$ tip dependence, and indeed we observe this dependence, again with minimal broadening until about 50° of tip.

In addition, we have examined the more general case, where in contrast to the above examples, the $v_z = 0$ zone does not lie in a constant $k_z = 0$ plane. This occurs in the (110) plane when the field is tipped out of plane from the ⟨110⟩ direction. In contrast to the (100)-plane data of Fig. 14 (where the in-plane dR/dH spectrum of Fig. 7 is merely stretched toward high fields as $1/\cos\theta$), the (110) in-plane spectrum of Fig. 9 changes markedly as the field is tipped. While the peak marked a in Fig. 9 moves as $1/\cos\theta$, two additional peaks split off from the double peak marked b and c which with reduced amplitude also moves as $1/\cos\theta$. The newly resolved peaks therefore do not follow the $1/\cos\theta$ variation. We ascribe these peaks to the $v_z = 0$ zones with nonconstant k_z located near the out-of-plane necks. It appears that tipping is a useful auxiliary means of identifying resonance signals in that it can distinguish different $v_z = 0$ zones.

VII. SURFACE CONDITIONS

In fitting the theory to the experimental traces, we have assumed that the electrons are always specularly reflected at the metal surface. The probability of diffuse reflection can however become appreciable when the metal surface is rough on a scale which is quite small compared with the depth of the trajectory. Such roughness results in readily identifiable line-shape changes.[1,2,23,24] In Cu a characteristic ground-state trajectory has a length $x_1 \approx 25\ \mu$, and a depth $z_1 \approx 0.1\ \mu$ which is on the order of the skin depth δ. In addition to the effect of diffuse scattering, we have observed two other distinct line-shape changes in the Cu due to surface imperfections. The three different types of surface perturbations are exemplified in parts (a), (b), and (c) of Fig. 15.

We consider first the regime where the characteristic length of the surface variation is large compared with z_1 and x_1, as in (a) of Fig. 15. We envision a gentle undulation of the sample surface. For $\omega\tau \approx 30$ an electron makes about five hops before being scattered by impurities or phonons so that it "sees" a curved surface with radius of curvature R_s. Such surface curvature induces a shift in the observed resonance position[15,25] by an amount $\Delta H = (\hbar/e)(K/R_s)$. R_s is not constant over the sample surface however; it takes on positive and negative values and ranges in absolute value from a minimum to infinity causing positive and negative peak position shifts from zero to a maximum value. The result is a broadening of all the peaks by a constant amount ΔH. This curvature broadening is the same for each peak, but the fractional broadening $\Delta H/H$ is most evident for the low-field transitions. Since peak amplitude is expected to vary inversely as the square of the fractional width, the curvature broadening has a marked effect on the peak amplitudes giving an increased damping toward zero field. A small amount of surface undulation is evident in even the best polished of our specimens, but when the orange-peel effect is pronounced the effect is readily evident—compare traces a and b in Fig. 16. There is a striking decrease in the relative amplitude of low- and high-field peaks. The measured ΔH in the figure is 0.5 Oe. To compare this value with that expected from the curvature field-shift relation, we need to estimate a representative value for R_s. The image of an object with dimension 1 cm reflected in the sample surface could just be resolved at 2-m distance so that [referring to Fig. 15(a)] $\theta \approx 0.005$. With the aid of a microscope we found λ [Fig. 15(a)] to be about 0.01 cm. This gives $R_s \approx 2$ cm. Together with the value of $K \approx 0.3 \times 10^8$ cm^{-1}, one would expect a broadening of about 0.9 Oe, not unlike the observed value.

The second regime of surface roughness is

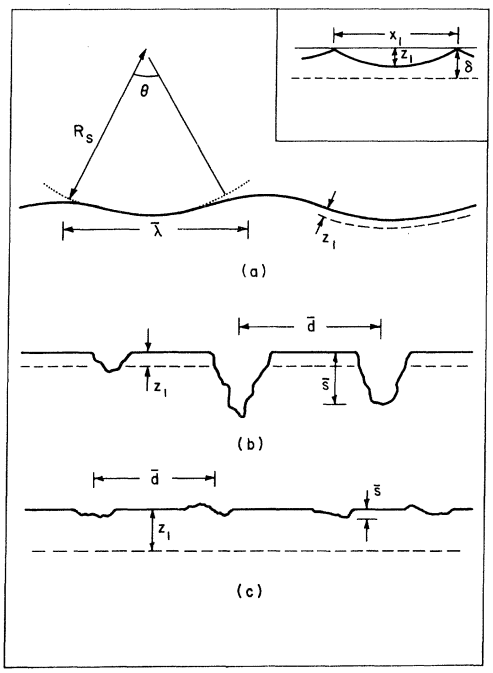

FIG. 15. Three types of surface roughness observed in the present experiments: (a) gentle undulation, (b) deep pitting, (c) shallow roughness. Insert: surface-electron trajectory and rf skin layer.

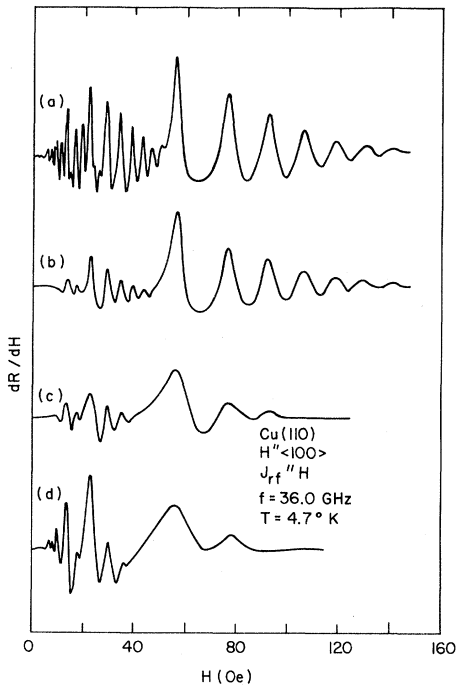

FIG. 16. Data characteristic of the three kinds of surface roughness. (a) "Best" surface, flat and not pitted. (b) Surface with gentle undulations giving curvature broadening. (c) Surface with deep pitting giving mean-free-path interruption. (d) Surface with shallow roughness giving diffuse surface scattering.

sketched in Fig. 15(b). We consider pits on the sample surface whose average depth $\bar{s}$ is greater than or on the order of the depth of the trajectory. These pits simply interrupt the trajectory and scatter the electrons. This "mean-free-path interruption" is expected to become noticeable when the average distance $\bar{d}$ between pits becomes less than the mean free path (mfp) in the absence of such pits. The resonance spectrum is expected to look just as if the temperature were raised or more impurities introduced into the sample, i.e., a decrease of $\omega\tau$. Trace (c) of Fig. 16 was observed on an occasion when the surface was badly pitted during polishing. A microscope picture revealed pits separated by something like 50 μ which represents roughly one-half an mfp, and indeed Γ^* values of traces (a) and (c) differ by about a factor of 2.

Finally, when the size of the surface perturbations becomes less than the trajectory depth [Fig. 15(c)], conventional diffuse surface scattering influences the line shape. While different estimates have been made of the power law,[1,2,23,26] it is generally agreed that the probability of diffuse scattering increases with increasing magnetic field. This effect has been illustrated by Koch and Murray in Ga and Sn and is also observed in the present Cu experiments. Only on rare occasion did we get a uniform and light tarnishing of the surface that showed the effect of surface scattering clearly. A beautiful example is shown in trace (d) of Fig. 16. [These data were not taken in the same sample as traces (a), (b), and (c).] The characteristic decay of the resonances toward high fields is clearly evident, and an electron microscope photograph of the sample surface revealed perturbations on the order of or less than 0.1 μ.

The experimental traces we have shown as examples of the three types of surface conditions are special. In general, combinations of the three effects can be present in a given trace. Although the curvature broadening is difficult to eliminate completely, with careful sample preparation it is not difficult to avoid surfaces like (b) and (c) of Fig. 15. The long polishing times used (ten or more hours for the best results) were necessary mainly to reduce the curvature broadening; 2 or 3 h were usually sufficient to obtain surfaces free of pitting. In addition, we found it best to mount the samples in the experimental apparatus immediately after polishing and to cool to liquid-nitrogen temperature in vacuum. This minimized the risk of subsequent corrosion and deterioration of the sample surface.

VIII. SUMMARY AND CONCLUDING COMMENTS

The present work aims to be an exemplary and comprehensive study of surface-electron resonances in Cu. By fitting observed spectra to calculations we provide for an accurate determination of the resonance fields. In order to extract from the data point-by-point values of the Fermi velocity, we have developed an iterative computation scheme that only requires knowledge of the FS geometry.

It appears that this iteration approach is applicable quite generally, although we cannot be sure that it would always converge rapidly enough to be practical. Nor is it certain that it always converges to a unique velocity distribution. For the specific case of velocities on the (100) and (110) central sections of Cu, we do arrive at values close to those due to Halse or Lee, yet sufficiently different to make for worthwhile comparison. In the course of the experiments, we have come to examine the tip dependence of the resonances to show that there are two distinctly different modes of tip variation in line with the recent theoretical considerations of Singhal and Prange. We also have observed and identified three characteristic kinds of surface perturbations, namely, curvature broadening, mean-free-path limitation by trajectory interruption and finally genuine diffuse surface scattering.

The over-all success of our experiments rests with the quality of surface polishing. The micro-

wave impedance of Cu has been studied in many previous experiments without a hint of the presence of surface electrons. In fact Pippard's studies[27] of the anomalous skin effect led him to conclude that electrons were scattered diffusely at the surface. In view of our observations, we must conclude that his surface preparation procedures were inadequate.

As a final note, we want to emphasize how important the calculation of the line shapes was for the accurate interpretation of the data. In view of this, it would be unwise to gloss over remaining discrepancies between theory and experiment. In reexamining the two curves of Fig. 5, some differences are apparent. The structure on the high-field side of the calculated $1 \rightarrow 2$ peak is not observed in the experiment. Only for high $\omega\tau$ values is this apparent. The fitted value of $\beta \approx 0.5$ is about 40% higher than that calculated from the known values of skin depth δ and curvature radius K, a discrepancy also noted in the case of Bi.[7]

The fact that the oscillations damp out more quickly in the experimental trace at low fields is due, we believe, to surface curvature broadening which we cannot eliminate entirely. Thus it should not be thought a significant deviation. The other shortcomings of the calculation may well lie with approximations employed in the theory. In particular, since the resonances are comparable in magnitude to cyclotron resonance signals in Cu, one may question whether the small-signal-limit consideration of NKP is strictly applicable here.

ACKNOWLEDGMENTS

We wish to acknowledge many pleasant and fruitful discussions with K. Sibbald and R. E. Prange concerning this work. We are indebted to B. DeSavage for making the electron microscope photographs that allowed us to examine sample surfaces in detail. Computer time was provided by the University of Maryland Computer Science Center.

[1]R. E. Prange and T. W. Nee, Phys. Rev. 168, 779 (1968).

[2]T. W. Nee, J. F. Koch, and R. E. Prange, Phys. Rev. 174, 758 (1968).

[3]J. F. Koch, in *Electrons in Metals*, edited by J. F. Cochran and R. R. Haering, Vol. I of *Solid State Physics* (The Simon Fraser University Lectures) (Gordon and Breach, New York, 1968).

[4]M. S. Khaikin, Advan. Phys. 18, 1 (1969).

[5]M. S. Khaikin, Zh. Eksperim. i Teor. Fiz. 391, 212 (1960) [Sov. Phys. JETP 12, 152 (1961)].

[6]J. F. Koch and C. C. Kuo, Phys. Rev. 143, 470 (1966).

[7]J. F. Koch and J. D. Jensen, Phys. Rev. 184, 643 (1969).

[8]J. F. Koch and R. E. Doezema, Phys. Rev. Letters 24, 507 (1970).

[9]W. J. Tegart, *The Electrolytic and Chemical Polishing of Metals in Research and Industry* (Pergamon, London, 1959).

[10]Amplitude is taken as the height of the peak measured from the minimum on the low-field side.

[11]M. H. Halse, Phil. Trans. Roy. Soc. London A265, 507 (1969); Ph.D. thesis (Cambridge University, 1967) (unpublished). For the (100) and (110) sample planes, Halse's seven-parameter equation may be written as a cubic equation in $\cos\frac{1}{2}ak$, where a is the lattice constant and k is any of the momentum-space coordinates k_x, k_y, and k_z.

[12]M. J. G. Lee, Phys. Rev. 187, 901 (1969).

[13]M. J. G. Lee, Phys. Rev. B 2, 250 (1970).

[14]J. F. Koch, R. A. Stradling, and A. F. Kip, Phys. Rev. 133, 240 (1964).

[15]R. E. Doezema, J. F. Koch, and U. Strom, Phys. Rev. 182, 717 (1969).

[16]An incorrect value of our neck velocity (due to an error in K_0) was communicated to Lee (Ref. 13).

[17]A. S. Joseph and A. C. Thorsen, Phys. Rev. 134, A979 (1964).

[18]V. S. Edelman and M. S. Khaikin, Zh. Eksperim. i Teor. Fiz. 49, 107 (1965) [Sov. Phys. JETP 22, 77 (1966)].

[19]B. Perrin, G. Weisbuch, and A. Libchaber, Phys. Rev. B 1, 1501 (1970).

[20]J. F. Koch and A. F. Kip, in *Proceedings of the Ninth International Conference on Low Temperature Physics, Columbus, Ohio,* 1964, edited by J. G. Daunt (Plenum, New York, 1965), pp. 818–822.

[21]R. T. Slivka and D. N. Langenberg, Bull. Am. Phys. Soc. 15, 90 (1970).

[22]S. P. Singhal and R. E. Prange, Phys. Rev. B 3, 4083 (1971).

[23]J. F. Koch and T. E. Murray, Phys. Rev. 186, 722 (1969).

[24]J. F. Koch, Physik Kondensierten Materie 9, 146 (1969).

[25]R. E. Prange, Phys. Rev. 171, 737 (1968).

[26]J. Mertsching and H. J. Fischbeck, Phys. Status Solidi 41, 45 (1970).

[27]A. B. Pippard, Phil. Trans. Roy. Soc. London A250, 325 (1957).